Applied Catalysis B: Environmental 228 (2018) 1–9

Contents lists available at ScienceDirect

Applied Catalysis B: Environmental

journal homepage: www.elsevier.com/locate/apcatb

Rational design of donor-π-acceptor conjugated microporous polymers for photocatalytic hydrogen production

Yunfeng Xu[a], Na Mao[a], Chong Zhang[a], Xue Wang[a], Jinghui Zeng[a], Yu Chen[a], Feng Wang[b], Jia-Xing Jiang[a,*]

[a] Key Laboratory for Macromolecular Science of Shaanxi Province, Shaanxi Key Laboratory for Advanced Energy Devices, School of Materials Science and Engineering, Shaanxi Normal University, Xi'an, Shaanxi, 710062, PR China
[b] Key Laboratory for Green Chemical Process of Ministry of Education, Wuhan Institute of Technology, Wuhan 430073, PR China

ARTICLE INFO

Keywords:
Conjugated microporous polymer
Donor-π-acceptor
Benzothiadiazole
Photocatalysis
Hydrogen evolution

ABSTRACT

Developing highly efficient catalysts for photocatalytic hydrogen generation from water splitting is one of the grand challenges in solar energy conversion. Herein, we report the design and synthesis of a library of donor-π-acceptor (D-π-A) conjugated microporous polymer (CMP) photocatalysts using pyrene, benzothiadiazole, and benzene (biphenyl) as donor, acceptor, and π crosslinker units, respectively. By adjusting the ratio of pyrene to benzothiadiazole units, a range of CMPs with various polymeric structures and components was synthesized and the influence of the molecular structures on the photocatalytic performance was comparatively investigated. Photocatalytic hydrogen evolution rate (HER) up to 106 μmol h^{-1} was achieved on PyBT-2 with a ratio of 9:2 of pyrene to benzothiadiazole under UV–vis light irradiation ($\lambda > 300$ nm). The structure-performance relationships revealed in this work offer a fundamental understanding in the rational design of CMPs for high performance organic photocatalysts.

1. Introduction

Hydrogen energy, as a green and sustainable energy system, has attracted much attention due to the higher calorific value and carbon-free emission upon combustion of hydrogen [1,2]. Photocatalytic hydrogen evolution from water splitting has been considered as a promising technology to address the energy crisis and environmental pollution [3–5]. In the past decades, most studies were mainly focused on inorganic metal-based semiconducting photocatalysts [6–9], which could absorb UV or visible light to generate electrons and holes. Particularly, significant advance has been achieved in carbon dots based semiconductor photocatalysts [10,11]. However, most inorganic photocatalytic materials suffer from low photocatalytic activity under visible-light, harsh preparation conditions, and rare elements [6]. Organic polymeric photocatalysts have been the subject of intense recent interest due to their diverse synthetic modularity, which allows the fine synthetic control over their chemical structures and electronic properties [12–16]. The linear conjugated polymers (*e.g.* poly(*p*-phenylene)s [17,18], poly(pyridine-2,5-diyl) [19,20]) showed moderate photocatalytic activity for hydrogen evolution from water under UV light irradiation [21]. Graphitic carbon nitride (g-C_3N_4), as the state-of-the-art organic photocatalyst, has been widely studied for hydrogen evolution from water splitting [22–26], and various synthetic strategies have been developed to improve the photocatalytic performance of g-C_3N_4 [27–29]. However, the synthesis of most g-C_3N_4 photocatalysts involves harsh preparation conditions and the real chemical structure is unknown, which limit the scope for fine-tuning chemical structure and electronic property [30–32].

Conjugated microporous polymers (CMPs) feature extended π-conjugation, high specific surface area, excellent physicochemical and thermal stability, tunable chemical structure and electronic property, making them attractive photocatalysts for hydrogen evolution [14,33–36]. Indeed, more recent studies revealed that CMPs are emerging as a novel class of photocatalysts for hydrogen production from water splitting and the photocatalytic activity could be improved by rational design of the polymer structure [13,14]. For example, Cooper et al. synthesized a series of pyrene-based CMPs photocatalysts with tunable optical gap, the obtained bare CMPs show highly photocatalytic activity for hydrogen evolution from water under visible-light irradiation [33]. They also developed the spirobifluorene-based CMPs with enhanced photocatalytic activity for hydrogen evolution under visible-light irradiation [37,38]. Yu et al. reported a series of bipyridyl-containing porous conjugated polymer photocatalysts and found that the photocatalytic activity could be greatly enhanced by improving

* Corresponding author.
E-mail address: jiaxing@snnu.edu.cn (J.-X. Jiang).

https://doi.org/10.1016/j.apcatb.2018.01.073
Received 1 November 2017; Received in revised form 22 January 2018; Accepted 29 January 2018
Available online 31 January 2018

charge separation processes and broadening light absorption because of the incorporation of bipyridyl unit [34,39]. Wang et al. developed a molecular structural design principle of conjugated polybenzodiazoles as organic photocatalysts for visible-light-promoted hydrogen evolution, and revealed that the linear conjugated polymer with an alternating phenyl-benzothidiazole polymer structure exhibited superior photocatalytic activity in H_2 evolution, compared to its three-dimensional polymer network counterparts [35]. We explored the influence of porosity, bandgap and charge transport on the photocatalytic performance of the perylene-containing CMPs photocatalysts [40,41]. Tian et al. prepared benzothiadiazole-based polymer dots organic photocatalysts, which also exhibited excellent photocatalytic activity for H_2 evolution from water splitting [42]. Beyond this, some other kinds of organic porous polymers with extended π-conjugation along the skeleton have also been developed for hydrogen evolution. For instance, the covalent triazine-based framework of CTF-T1 with π-stacked aromatic units showed excellent photocatalytic activity for hydrogen evolution under visible light irradiation [43]. The 2D imine-linked covalent organic framework of TFPT-COF with strong light harvesting capability also exhibited great potential for photocatalytic hydrogen generation under visible light irradiation [44]. Considering the synthetic diversity, flexible design ability and the variety of structural variations of CMPs, one could expect to develop more efficient CMPs photocatalysts for hydrogen evolution by the rational molecular design.

In this work, we constructed a library of donor-π-acceptor (D-π-A) CMPs photocatalysts and demonstrated their high photocatalytic performance for hydrogen evolution. Pyrene with planar structure and extended π-conjugation was employed as donor unit, the electron-withdrawing benzothiadiazole was selected as acceptor unit, and benzene or biphenyl was used as π crosslinker unit, respectively. The influences of molecular structure and the ratio of donor to acceptor on the photocatalytic performance of the resulting CMPs were comparatively studied. It was found that the photocatalytic performance of the D-π-A polymers is much better than that of the D-A alternatively polymers without π crosslinker unit and the D-π-D polymers without acceptor unit. Additionally, the ratio of donor to acceptor has a large influence on the photocatalytic performance of the resulting CMPs photocatalysts. This work highlights that the construction of D-π-A is crucial for the rational design of efficient CMPs photocatalysts.

2. Experimental section

2.1. Chemical and materials

Pyrene, bromine, 1,4-benzenediboronic acid, 4,7-dibromobenzothiadiazole, bis(pinacolato)diboron, [1,1′-bis(diphenylphosphino)ferrocene]dichloropalladium(II) ($Pd(dppf)Cl_2$), potassium acetate and potassium carbonate were purchased from TCI. Tetrakis(triphenylphosphine)palladium(0) ($Pd(PPh_3)_4$), dioxane, tetrahydrofuran (THF), nitrobenzene and *N*,*N*-dimethylformamide (DMF) were purchased from J&K Scientific Ltd. All chemicals were used as received without further purification. 1,3,6,8-Tetrabromopyrene, 2,1,3-benzothiadiazole-4,7-bis(boronic acid pinacol ester) and 3,5,3′,5′-tetrakis(4,4,5,5-tetramethyl-1,3,2-dioxaborolan-2-yl)biphenyl were synthesized according to the reported methods [45–47].

2.2. Synthesis of the polymers

All the polymers were synthesized *via* Pd(0)-catalyzed Suzuki－Miyaura coupling reaction. A typical experimental procedure for PyBT-0 is given as an example. To a mixture of 1,4-benzenediboronic acid (322 mg, 2.0 mmol) and 1,3,6,8-tetrabromopyrene (518 mg, 1.0 mmol) in DMF (25 mL), an aqueous solution of K_2CO_3 (2.0 M, 5 mL) and $Pd(PPh_3)_4$ (10 mg, 8.6 μmol) were added. The mixture was degassed under freeze–pump–thaw, purged with N_2, and stirred at 150 °C for 48 h. Then, the mixture was cooled to room temperature and poured into water. The precipitate was collected by filtration, and washed with water, chloroform, tetrahydrofuran and methanol, respectively. Further purification of the polymer was carried out by Soxhlet extraction with tetrahydrofuran for 72 h. The product was dried in vacuum for 24 h at 70 °C and obtained as a green-yellow powder (Yield: 345 mg, 98%). Elemental combustion analysis (%) Calcd for $(C_{28}H_{14})_n$: C, 96%; H, 4%; Found C, 93.36%; H, 4.88%; Pd 0.000154% from ICP-MS. The detail of the synthesis for the other polymers is given in the Supporting Information.

2.3. Characterization

FT-IR spectrum was measured on a Tensor 27 FT-IR spectrometer (Bruker) in transmission mode at room temperature. Solid state magic angle spinning ^{13}C CP/MAS NMR measurement was carried out on a Bruker Avance III model 400 MHz NMR spectrometer at a MAS rate of 10 kHz. Thermal properties of the polymer networks were evaluated using thermogravimetric analysis (TGA) with a differential thermal analysis instrument (Q1000DSC + LNCS + FACS Q600SDT) over the temperature range from 30 to 800 °C under a nitrogen atmosphere with a heating rate of 10 °C min^{-1}. Morphology of the polymer networks was obtained using a field emission scanning electron microscope (SEM, JSM-6700F, JEOL, Japan). Powder X-ray diffraction measurement was carried out on an X-ray Diffractometer (D/Max-3c). Elemental analysis was performed on a EURO EA3000 Elemental Analyzer. Pd content was determined by inductively coupled plasma mass spectrometry (ICP-MS), where the sample (25 mg) was firstly digested in HNO_3/H_2O_2 (0.8 mL/0.2 mL) at 60 °C for 12 h, then cooled to room temperature and diluted with HNO_3 (4 mL). Surface areas and pore size distributions were measured by N_2 adsorption and desorption at 77.3 K using an ASAP 2420-4 (Micromeritics) volumetric adsorption analyzer. Surface area was calculated in the relative pressure (P/P_0) ranging from 0.05 to 0.20. Pore size distributions and pore volumes were derived from the N_2 adsorption branch using non-local density functional theory (NL–DFT). Sample was degassed at 120 °C for 12 h under vacuum (10^{-5} bar) before analysis. UV–vis diffuse reflection spectrum was obtained for the dry-pressed disk samples using a scanning UV–vis spectrophotometer (UV-Lambda 950, PerkinElmer, US) equipped with an integrating sphere assembly, using $BaSO_4$ as a reflectance sample. Fluorescent spectrum of the polymers was measured with a Shimadzu F-7000 PC fluorescence spectrometer by using excitation wavelength of 400 nm at room temperature. Time-resolved fluorescence spectroscopy was performed on Edinburgh Instruments FLS 920 fluorescence spectrometer.

2.4. Electrochemical measurements

Cyclic voltammetry (CV) measurement was carried out on a CHI660E (Chenhua, Shanghai) electrochemical workstation in a three-electrode-cell system: glassy carbon electrode as the working electrode, $Hg/HgCl_2$ electrode as the reference electrode, platinum wire as the counter electrode. The sample was prepared by first mixing ground polymer with 5 wt% Nafion, the mixture was dropped cast on top of a glassy carbon working electrode and let the solvent evaporate in a vacuum chamber for 60 min. The measurement was carried out in a solution of tetrabutylammonium hexafluorophosphate (0.1 M) as supporting electrolyte in acetonitrile with a scan rate of 100 mV s^{-1} in the range of –1.6 V to 1.2 V. For the conversion from $Hg/HgCl_2$ redox couple to the Normal Hydrogen Electrode (NHE), the equation of $E_{NHE} = E_{SCE} - 0.241$ V was applied. Three times were carried out for each sample to get an average value. The photocurrent of the polymer was measured on CHI660E electrochemical workstation with a bias voltage of 0.02 V under UV–vis light irradiation with 20 s light on-off cycles. The working electrode prepared from the polymer catalyst and 5 wt% Nafion was immersed in 0.1 M Na_2SO_4 aqueous solution.

2.5. Photocatalytic performance measurement

The hydrogen evolution experiment was performed on a LabSolar-III AG reaction cell (Beijing PerfectLight Co.). 100 mg polymer photocatalyst was suspended in 100 mL triethanolamine aqueous solution (20 vol% v/v). All photocatalytic experiments were performed in a double-walled glass reactor, where the outer compartment is circulated with water to keep a constant temperature (25 °C) through a thermostat. The suspension was thoroughly degassed to remove air and irradiated using a 300 W Xe lamp (PLS-SEX300/300UV, Beijing PerfectLight Co.). A cut off filter (Kenko L-42) was employed to achieve visible-light ($\lambda > 420$ nm). The yield of hydrogen was determined by using an online gas chromatograph (GC7900, Techcomp) equipped with a column of 5 Å molecular sieves and a thermal conductivity detector, and nitrogen was used as the carrier gas. The oxygen evolution experiment was also performed on a LabSolar-III AG reaction cell (Beijing PerfectLight Co.). 100 mg polymer powder was suspended in an aqueous solution (100 mL) containing $Co(NO_3)_2{\cdot}6H_2O$ (0.29 g, 0.01 M) as an electron acceptor and La_2O_3 (0.1 g) as a pH buffer agent. The solution was evacuated several times to completely remove air prior to irradiation under a 300 W Xe lamp. The yield of oxygen was determined by using an online gas chromatograph (GC7900, Techcomp) equipped with a column of 5 Å molecular sieves and a thermal conductivity detector, and argon was used as the carrier gas.

3. Results and discussion

A library of D-π-A CMPs photocatalysts was synthesized *via* statistical polymerization using Pd(0)-catalyzed Suzuki − Miyaura coupling reaction (Scheme 1). The component of the resulting polymers could be adjusted by the feed ratio of 1,3,6,8-tetrabromopyrene to 4,7-dibromobenzothiadiazole. Benzene and biphenyl were used as π crosslinker units for the polymers of series–1 and series–2, respectively. All of the polymers are firstly reported here except for the polymer PyBT-0, which was reported as CP-CMP10 previously [33]. Thermogravimetric analysis revealed that the polymers have a high thermal stability in nitrogen atmosphere ($T_d > 500$ °C, Fig. S1). FT-IR spectra confirmed the polymer structures, as evidenced by the characteristic peaks of benzothiadiazole unit at around 1610, 1590 and 753 cm^{-1} (Fig. S2, 3). The solid-state ^{13}C NMR spectra of the polymers showed broad peaks ranging from 122 to 164 ppm (Fig. 1), corresponding to the signals of aromatic carbons. The characteristic carbon signals from benzothiadiazole unit could be clearly observed at 160 ppm for the benzothiadiazole-containing polymers, which was not observed in the solid-state NMR spectra of PyBT-0 and PhBT-0 without benzothiadiazole unit, further confirming the polymer structure. Elemental analysis of the CMP photocatalysts supports the structures as proposed (Table S1). Powder X-ray diffraction measurements indicated that all of the polymers are amorphous in nature (Fig. S4), as observed for the reported CMPs [33–35,48,49]. All the resulting polymers show very similar morphology with relatively uniform solid nanospheres, as revealed by scanning electron microscopy (Fig. S5).

Nitrogen adsorption and desorption isotherms analysis demonstrated that most of the polymer networks are porous, while the polymers of PyBT-5, PyBT-6 and PhBT-10 with high benzothiadiazole content are almost non-porous (Fig. S6, 7; Table S2). The apparent Brunauer–Emmet–Teller specific surface area shows an overall down trend with increasing benzothiadiazole content in both series − 1 and series − 2 (Table 1), which is possibly attributed to the decreased crosslinked degree of the polymers because of the less connectivities of benzothiadiazole (two active positions) compared with pyrene unit (four active positions) as shown in Scheme 1. The optical property and band gap of the prepared polymer networks were investigated by combining UV–vis diffuse reflectance spectroscopy, photoluminescence spectroscopy and cyclic voltammetry (CV) measurements. The UV–vis diffuse reflectance spectra of the polymer networks showed a broad light absorption in the visible region and a redshift trend with increasing of benzothiadiazole content in both series–1 and series–2 (Fig. 2a, b). PhBT-0 without benzothiadiazole unit shows the narrowest absorption range, while PyBT-7 with the highest benzothiadiazole content exhibits the broadest light adsorption range among the polymers in series–1. Similar result was also observed for the polymers in series–2. Optical gap as derived from the absorption edges varied between 2.44 eV (for PyBT-0) and 2.06 (for PyBT-7) in series–1 (Table 2). As for the polymers in series–2, PhBT-0 without benzothiadiazole unit shows the broadest band gap of 2.46 eV, while PhBT-7 with the highest benzothiadiazole content possesses the narrowest optical gap of 2.17 eV. CV measurement was carried out to further study the energy band structures of the polymer networks (Fig. S8, 9). The results revealed that all of the polymers possess high enough the lowest unoccupied molecular orbital (LUMO) energy level for the proton reduction half-reaction from water-splitting (Fig. 2c, d), although no straightforward correlation was observed between LUMO energy level and the benzothiadiazole content for these polymers, as observed for other reported benzothiadiazole-containing CMPs [35]. All of the polymers show strong solid state fluorescence. PyBT-0 without benzothiadiazole unit shows a maximum characteristic emission at 529 nm (Fig. S10a). By contrast, the photoluminescence spectra of the polymers with benzothiadiazole units (PyBT-1 to PyBT-7) show a gradual redshift from 545 nm for PyBT-1 to 591 nm for PyBT-7 with increasing of benzothiadiazole content. The same trend was observed for the polymers in series–2 (Fig. S10b), which is in good line with the UV–vis adsorption spectra. These results demonstrated that the optical properties and electronic structures of these polymer networks could be finely tuned by adjusting the ratio of donor (pyrene) to acceptor (benzothiadiazole) units.

Photocatalytic hydrogen evolution experiments were carried out with these polymers in the presence of a sacrificial electron donor. Triethanolamine (TEOA) was selected as sacrificial agent since it shows the highest photocatalytic activity in this system for the tested sacrificial agents (Fig. S11). The photocatalytic activity of the polymers was initially evaluated by using these bare polymers as unprocessed powders in water containing 20 vol% TEOA under UV–vis light irradiation ($\lambda > 300$ nm). Steady hydrogen production was observed with all of the as-prepared polymers under UV–vis light irradiation within 8 h (Fig. 3a, b). PyBT-0 without the acceptor unit of benzothiadiazole shows a moderate average hydrogen evolution rate (HER) of 27.7 μmol h^{-1}, while the photocatalytic activity of the D-π-A polymers (PyBT-1 to PyBT-6) increased firstly and then decreased with the increasing of benzothiadiazole content (Fig. 3a). PyBT-2 with a ratio of 9:2 of pyrene to benzothiadiazole shows the highest HER of 52.5 μmol h^{-1} in the polymers of series–1, which is much higher than those of the D-A alternatively polymer PyBT-7 (5.4 μmol h^{-1}) without π crosslinker of benzene and the D-π-D polymer PyBT-0 (27.7 μmol h^{-1}) without benzothiadiazole acceptor unit. Similar result was also observed for the polymers in series–2, where PhBT-4 with a ratio of 6:8 of pyrene to benzothiadiazole shows the highest HER of 47.1 μmol h^{-1} (Fig. 3b). This value is also much higher than those of the D-π-D polymer PhBT-0 (15.5 μmol h^{-1}) without the benzothiadiazole acceptor unit and the π-A polymer PhBT-10 (0.95 μmol h^{-1}) without the pyrene donor unit. These results demonstrate that the construction of D-π-A polymers promotes effectively the charges transporting and separation between hole and electron because of the co-existence of donor unit of pyrene and acceptor unit of benzothiadiazole in a polymer chain, leading to the enhanced photocatalytic performance of the polymers. In addition, the ratio of donor to acceptor is also an important variable to balance the hole and electron transporting. The reason for the relatively lower photocatalytic activity of the polymers in series–2 compared with series–1 may originate from the twisted biphenyl unit. The polymers in series–1 consist of planar phenyl crosslinker facilitating the charges transporting, whereas the twisted biphenyl crosslinker in the series–2 polymers may block the charges transporting. The high hydrogen

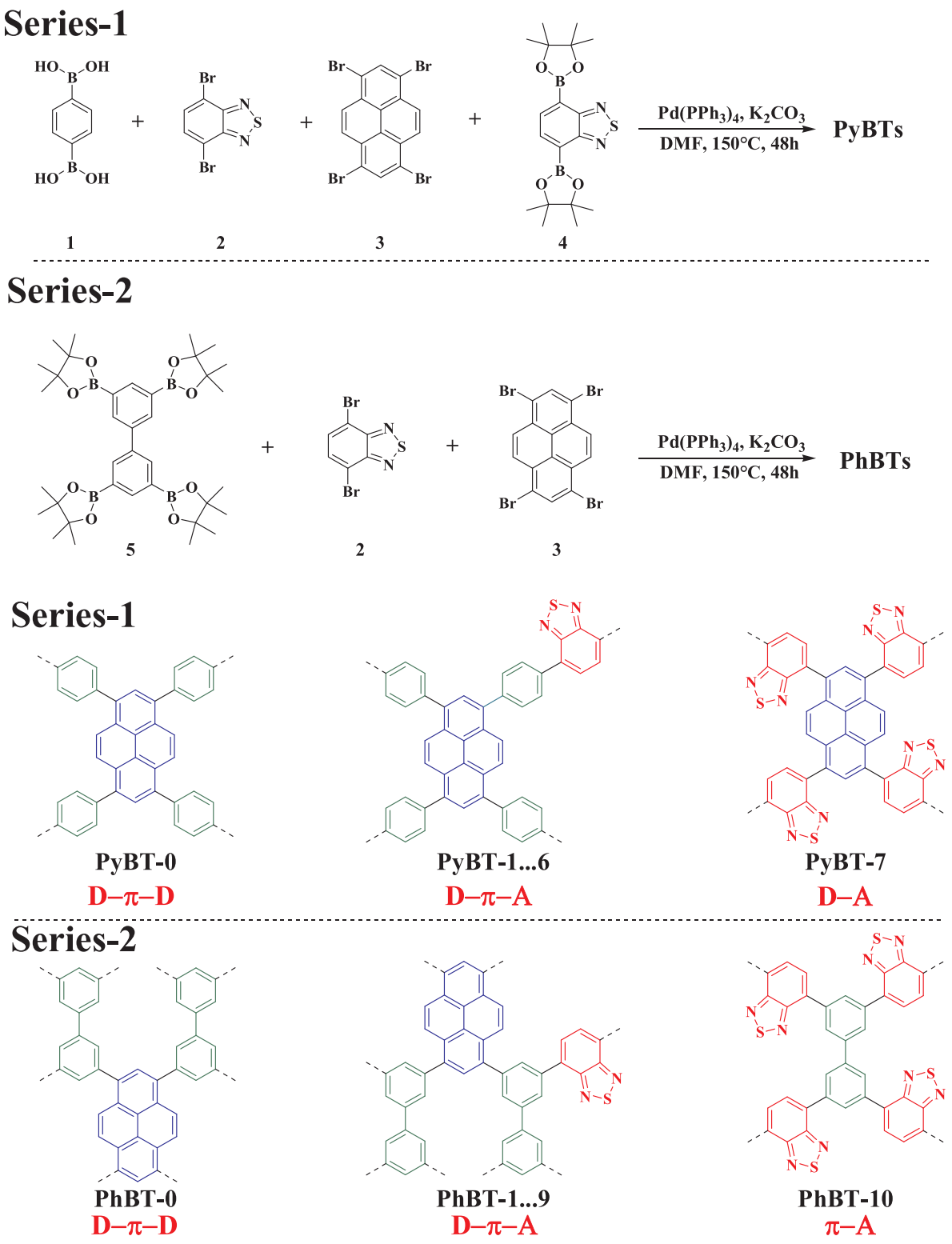

Scheme 1. Synthetic routes to the polymers and the notional polymer structures.

evolution activity of the D-π-A polymers could be evidenced by the time-resolved fluorescence spectroscopy and the photocurrent measurement. It was found that the D-π-A polymer PyBT-2 shows much shorter fluorescence lifetime (τ_1 = 0.19 ns, τ_2 = 1.18 ns) than the D-π-D polymer PyBT-0 (τ_1 = 0.41 ns, τ_2 = 1.81 ns), the D-A polymer PyBT-7 (τ_1 = 0.76 ns, τ_2 = 2.84 ns), and even the D-π-A polymer PhBT-4 (τ_1 = 0.38 ns, τ_2 = 1.73 ns) (Fig. S12), indicating the lower inactivation ratio of the excited state in PyBT-2, which benefits to the photocatalytic reduction reaction of water [40,41]. In addition, the photocurrent measurement also demonstrated that the D-π-A polymer PyBT-2 has much stronger transient photocurrent than the D-π-D polymer PyBT-0 and D-A polymer PyBT-7 (Fig. S13a). Similar result was also observed for the polymers in series–2 with enhanced transient photocurrent in the D-π-A polymer PhBT-4 (Fig. S13b). These results further demonstrated that the D-π-A polymers, particularly for PyBT-2, have improved light-induced electronic conductivity, and efficient charge transfer and

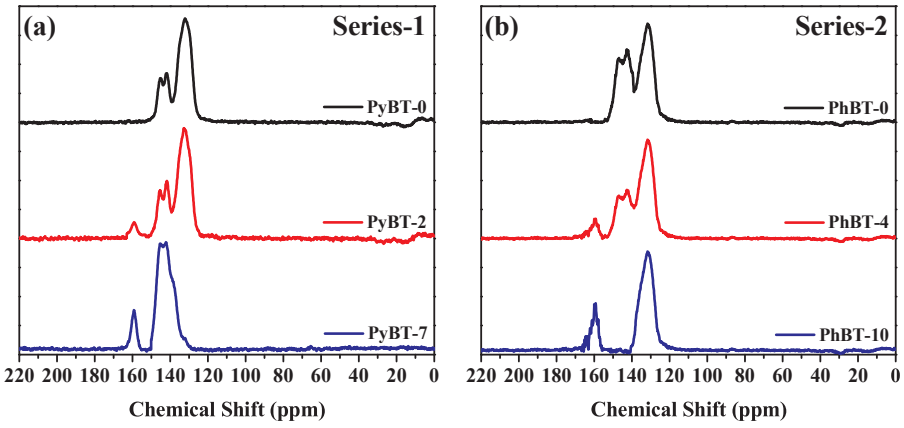

Fig. 1. The representative solid-state ^{13}C CP/MAS NMR spectra of the polymers (a: Series–1; b: Series–2).

Table 1
Monomer feed ratio and surface area of the polymers.

Polymers	relative molar monomer ratio					S_{BET}[a] [$m^2 g^{-1}$]
	1	2	3	4	5	
PyBT-0	2.0	0	1.0	0	0	871
PyBT-1	2.0	0.1	0.95	0	0	617
PyBT-2	2.0	0.2	0.9	0	0	865
PyBT-3	2.0	0.4	0.8	0	0	542
PyBT-4	2.0	0.6	0.7	0	0	324
PyBT-5	2.0	0.8	0.6	0	0	46
PyBT-6	2.0	1.0	0.5	0	0	27
PyBT-7	0	0	1.0	2.0	0	248
PhBT-0	0	0	1.0	0	1.0	1204
PhBT-1	0	0.2	0.9	0	1.0	1201
PhBT-2	0	0.4	0.8	0	1.0	1152
PhBT-3	0	0.6	0.7	0	1.0	1111
PhBT-4	0	0.8	0.6	0	1.0	930
PhBT-5	0	1.0	0.5	0	1.0	738
PhBT-6	0	1.2	0.4	0	1.0	712
PhBT-7	0	1.4	0.3	0	1.0	497
PhBT-8	0	1.6	0.2	0	1.0	386
PhBT-9	0	1.8	0.1	0	1.0	375
PhBT-10	0	2.0	0	0	1.0	32

[a] Surface area was calculated from N_2 adsorption isotherm in the relative pressure (P/P_0) range from 0.05 to 0.20.

charge separation in the polymer backbone because of the nature of D-π-A polymer structure, which lead to the improvement of photocatalytic performance for the D-π-A polymer.

It was reported that Pd catalyst residues could contribute the photocatalytic hydrogen evolution [38]. However, the residual palladium (Pd) content in these polymers are very low (< 7 ppm), as revealed by ICP-MS measurement. It was found that the Pd content increases gradually with the increasing of benzothiadiazole content (Table S1), which might be due to the strong coordination effect between heteroatoms (*e.g.* sulfur and nitrogen atoms from benzothiadiazole unit) and Pd. There is no linear relationship between the residual Pd and the photocatalytic performance in the two series CMP photocatalysts, indicating that the residual Pd has no significant effect on the hydrogen production rate in these polymers, as observed in other CMP photocatalysts [33–35,50]. Many reports have revealed that platinum (Pt) is one of the state-of-art noble metal cocatalysts for photocatalytic hydrogen evolution [34,35,40,51,52]. To further probe the effect of noble-metal cocatalysts, we tested the photocatalytic performance of the polymers with Pt cocatalyst *via* photo-deposition method from H_2PtCl_6. All of the polymers show enhanced photocatalytic performance when 3 wt% Pt was added as cocatalyst (Fig. 3c, d), which could be attributed to the improved electron localization from the conduction band of the polymer to the deposited Pt nanoparticles surface [53–55]. The photocatalytic performance of the polymers with 3wt% Pt also increased firstly and then decreased with the increasing of benzothiadiazole content (Fig. 4a). For example, PyBT-2 with 3 wt% Pt shows a maximum HER of 106.2 μmol h^{-1} among the polymers in series–1, and a maximum HER of 86.2 μmol h^{-1} for PhBT-4 was obtained in series–2 photocatalysts, indicating the importance of the content of benzothiadiazole for improving photocatalytic performance of the D-π-A polymers.

It is noteworthy that the hydrogen production rate of 106.2 μmol h^{-1} for PyBT-2 is higher than those of many other reported organic photocatalysts, such as poly(*p*-phenylene) (3.0 μmol h^{-1}) [18], poly-(phenyleneethynylene) (1.0 μmol h^{-1}) [56], poly(azomethine) (7.0 μmol h^{-1}) [57], PCP2-100%PDI (7.2 μmol h^{-1}) [50], perylene-based CMP of PrCMP-3 (12.1 μmol h^{-1}) [40], spirobifluorene-containing CMP of PCP2e (26 μmol h^{-1}) [34], SP-CMP (28.8 μmol h^{-1}) [37], donor-acceptor porous conjugated polymer of PCP6 (59.8 μmol h^{-1}) [39], and benzothiadiazole-containing polymer network of B-BT-0.05 (82 μmol h^{-1}) [35]. But it is still low in comparison with other organic photocatalysts with one-dimensional (1D) polymer structure, such as the linear benzothiadiazole-containing polymer of B-BT-1,4 (116 μmol h^{-1}) [35] and the dibenzo[b,d]thiophene-based linear conjugated polymer photocatalyst of P7 (145 μmol h^{-1}) [38]. The main reason might be attributed to the crosslinked polymer structure of these CMPs photocatalysts is not good for the charge transfer compared with the 1D polymer structure of the linear organic photocatalysts [35].

The photocatalytic hydrogen production property of the polymer photocatalysts under visible light irradiation was also investigated by using a long-pass filter that only transmits visible light ($\lambda > 420$ nm). All of the polymers show reduced photocatalytic activity under visible light irradiation (Fig. S14, 15), indicating that the ultraviolet light (300 nm < λ < 420 nm) mainly contribute to the photocatalytic activity in these polymers, although the polymers could absorb a broad range of light from 300 to 600 nm. The photocatalytic activity of these polymers under visible light could be improved by the preparation of heterojunction composite photocatalysts *via* a facile *in-situ* polymerization of CMPs and inorganic semiconductor [58–60]. For understanding the interplay between the photocatalytic activity and the light absorption of these polymer photocatalysts, the wavelength-dependent apparent quantum yield (AQY) of the two most efficient CMP photocatalysts (PyBT-2 and PhBT-4) was further investigated. It was found that the AQY decreases with increasing the wavelength of the incident light (Fig. S16), which matches well with that of the light absorption in the optical spectra of the polymers, suggesting that the reaction proceeds through light absorption within these polymer photocatalysts.

The photocatalytic mechanism of the D-π-A polymers mainly includes light adsorption, photo-induced electron-hole pairs, charge carriers transport and separation, and surface adsorption and redox reaction, which are intimately associated with the intrinsic characteristics of the polymers [5,61–63]. The porous structure of the D-π-A polymers

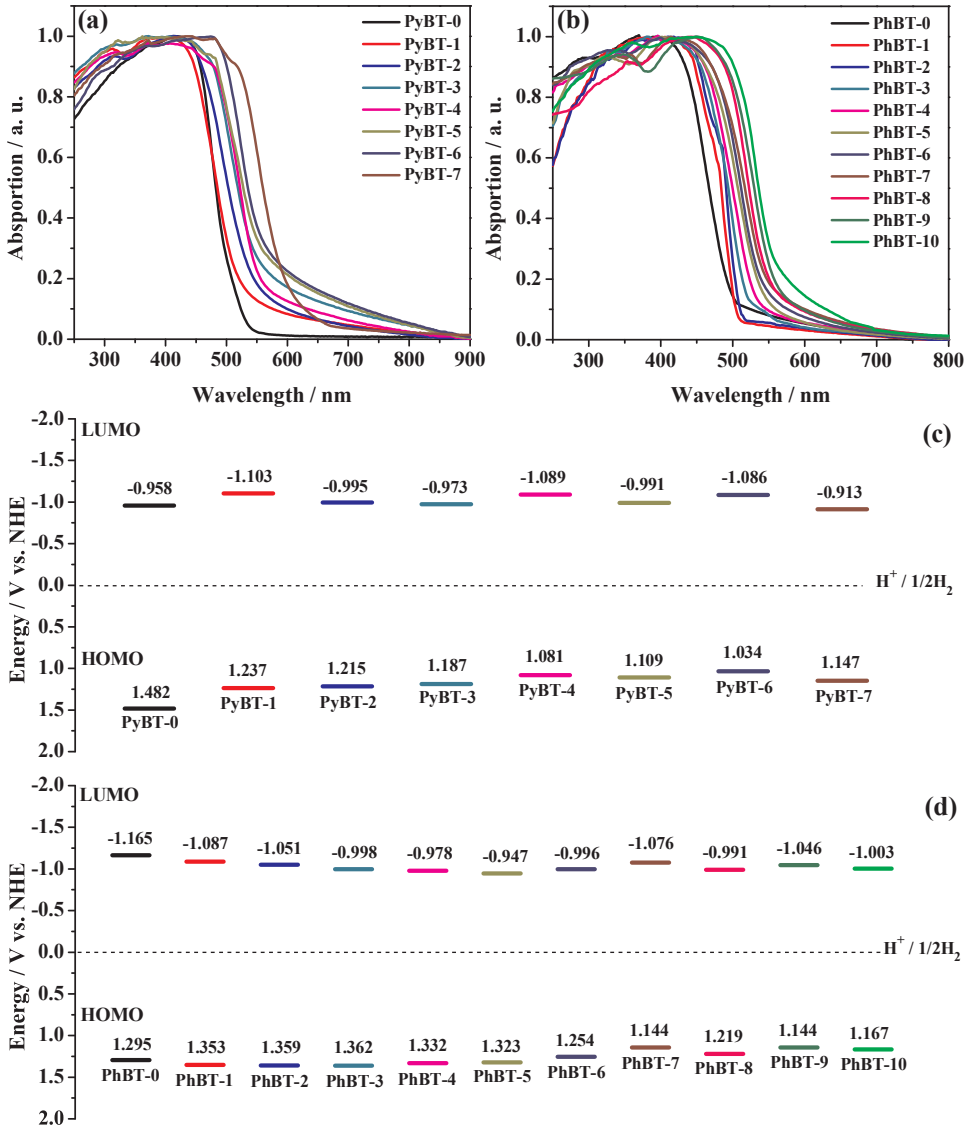

Fig. 2. (a) UV–vis absorption spectra of series–1 measured in the solid state; (b) UV–vis absorption spectra of series–2 measured in the solid state; (c) The highest occupied molecular orbital (HOMO) and the lowest unoccupied molecular orbital (LUMO) band positions of series–1; (d) HOMO and LUMO band positions of series–2 (the standard error of LUMO position is ± 0.005 eV from three measurements).

can increase the light path by the multiple scattering effect, leading to more light harvesting to photo-generate electron-hole pairs. The extended π-conjugation along the polymer skeleton promotes the migration of charges from the bulk to the surface of the polymer. The nature of D-π-A structure facilitates the separation of electrons and holes because of the electron push-pull effect of the donor and acceptor units. The high surface area of the polymers can provide abundant accessible surface for reactants as well as plentiful photocatalytic active sites. As a result, the D-π-A polymers with optimized polymer structure (*e.g.* the ratio of donor to acceptor) show improved photocatalytic performance owing to the synergetic effect of the above mentioned factors.

The cycling stability of PyBT-2 as an example was evaluated in a continuous photocatalytic reaction for 30 h with intermittent evacuation every 6 h under UV–vis light irradiation. As shown in Fig. 4b, a linear relationship between the produced hydrogen amount and reaction time was observed for each photocatalytic cycle. No significant decrease in photocatalytic activity of PyBT-2 was observed when the sample was subjected to five consecutive photocatalytic runs over a period of 30 h, indicating that the polymer has excellent photocatalytic stability under UV–vis light irradiation. After 30 h photocatalytic reaction, the recovered PyBT-2 was also carried out by FT-IR, UV–vis absorption and photoluminescence spectra, powder X-ray diffraction, N_2 adsorption − desorption, and SEM and TEM measurements (Fig. S17–20), the results revealed that PyBT-2 could maintain its structure well after photocatalytic reaction, which allows for PyBT-2 excellent photocatalytic recycling stability. In addition, small Pt nanoparticles were found to be deposited on the polymer surface after photocatalytic reaction as evidenced by the TEM measurement (Fig. S20c, d). In order to test the repeatability of the polymers, the other four batches of PyBT-2 were synthesized under the same conditions. All the samples show very similar surface area and pore structure based on nitrogen adsorption − desorption analysis (Fig. S21, Table S3). The photocatalytic experiment revealed that the HER of the bare samples without Pt cocatalyst varied between 51.6 and 60.2 μmol h^{-1} under UV–vis light irradiation (Fig. S22), and it increased to the range of 103–123 μmol h^{-1} when 3 wt% Pt was added (Fig. 4c). Such small difference in photocatalytic activity demonstrated that PyBT-2 has a good reproducibility from batch to batch.

The photocatalytic oxygen evolution activity of the D-π-A polymer was also evaluated by using PyBT-2 as an example. No any detectable oxygen could be observed when the bare PyBT-2 was irradiated by UV–vis light ($\lambda > 300$ nm) for 8 h in pure water without any electron scavenger or oxidation cocatalyst. In contrast, steady oxygen production was observed when $Co(NO_3)_2$ as the electron scavenger and La_2O_3 as the pH buffer agent were added into the reaction mixture (Fig. S23), and a moderate average oxygen evolution rate of 57.9 μmol h^{-1} was achieved. The enhanced oxygen evolution activity could be explained by the cobalt cocatalysts could serve as charge carrier trap centers to

Table 2
Photophysical property and hydrogen evolution rate for the CMP photocatalysts.

Polymers	λ_{em}[a] (nm)	LUMO[b] (eV)	optical gap[c] (eV)	HOMO[d] (eV)	HER[e] (μmol h^{-1})	HER[f] (μmol h^{-1})	HER[g] (μmol h^{-1})
PyBT-0	529	–0.958	2.44	1.482	27.7	37.4	20.9
PyBT-1	545	–1.103	2.34	1.237	31.7	53.2	18.8
PyBT-2	546	–0.995	2.21	1.215	52.5	106.2	29.6
PyBT-3	558	–0.973	2.16	1.187	23.4	41.8	17.1
PyBT-4	559	–1.089	2.17	1.081	16.6	29.6	12.5
PyBT-5	557	–0.991	2.10	1.109	13.7	25.3	9.2
PyBT-6	558	–1.086	2.12	1.034	9.2	14.5	4.6
PyBT-7	591	–0.913	2.06	1.147	5.4	9.6	2.8
PhBT-0	504	–1.165	2.46	1.295	15.5	32.1	7.1
PhBT-1	521	–1.087	2.44	1.353	16.1	26.9	9.1
PhBT-2	528	–1.051	2.41	1.359	23.6	43.1	12.1
PhBT-3	531	–0.998	2.36	1.362	38.6	67.6	20.4
PhBT-4	536	–0.978	2.31	1.332	47.1	85.2	22.8
PhBT-5	539	–0.947	2.27	1.323	31.1	56.1	15.6
PhBT-6	545	–0.996	2.25	1.254	21.8	42.1	10.8
PhBT-7	546	–1.076	2.22	1.144	13.2	22.9	7.7
PhBT-8	549	–0.991	2.21	1.219	8.6	16.4	4.9
PhBT-9	551	–1.046	2.19	1.144	6.8	12.5	2.4
PhBT-10	555	–1.003	2.17	1.167	0.95	1.7	0.5

[a] Photoluminescent emission peak of the polymer recorded in the solid state.
[b] LUMO energy level measured by CV.
[c] Calculated from the absorption edge.
[d] Calculated from optical gap and CV; Photocatalytic reaction conditions.
[e] 100 mg polymer was suspended in 100 mL triethanolamine/water solution (20 vol%) and irradiated by UV–vis light (λ > 300 nm).
[f] 100 mg polymer with 3 wt% Pt was suspended in 100 mL triethanolamine/water solution (20 vol %) and irradiated by UV–vis light (λ > 300 nm).
[g] 100 mg polymer with 3 wt% Pt was suspended in 100 mL triethanolamine/water solution (20 vol%) and irradiated by visible light (λ > 420 nm).

promote charges migration from the bulk to the interface of the polymer, reducing the recombination probability of the photo-induced electrons and holes [64]. Although the present preliminary results demonstrate that the D-π-A polymer is promising organic photocatalyst for oxygen evolution, the mechanism of oxygen evolution and the optimization of photocatalytic reaction conditions are needed to be further studied. Our fellow-up work will focus on these issues.

4. Conclusions

A library of D-π-A CMPs with varied ratio of pyrene to benzothiadiazole was synthesized and the photocatalytic performance for hydrogen evolution from water was explored. Our comparative study on the photocatalytic performance of the structure-designed CMPs photocatalysts revealed that the D-π-A molecular structure, species of the π crosslinker, and the ratio of the donor to acceptor play significant roles

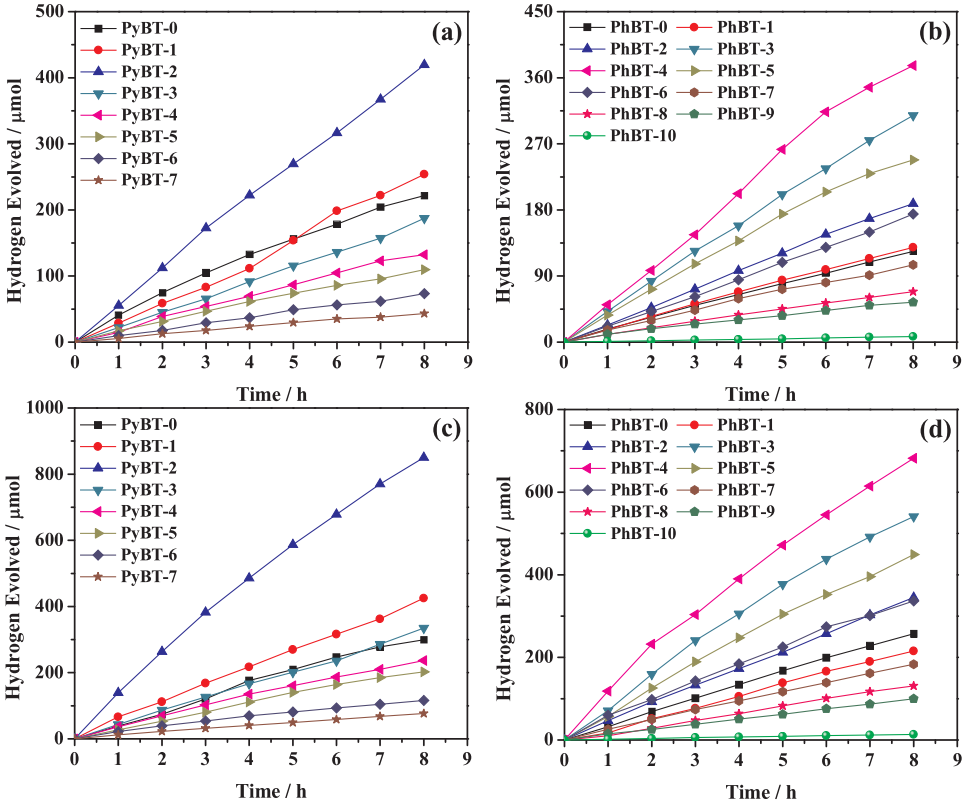

Fig. 3. Time course of hydrogen evolution of the bare CMP photocatalysts from water containing 20 vol% triethanolamine under UV–vis light irradiation (λ > 300 nm): (a) series–1, (b) series–2; Time course of hydrogen evolution of the CMP photocatalysts with 3 wt% Pt from water containing 20 vol% triethanolamine under UV–vis light irradiation (λ > 300 nm): (c) series–1, (d) series–2.

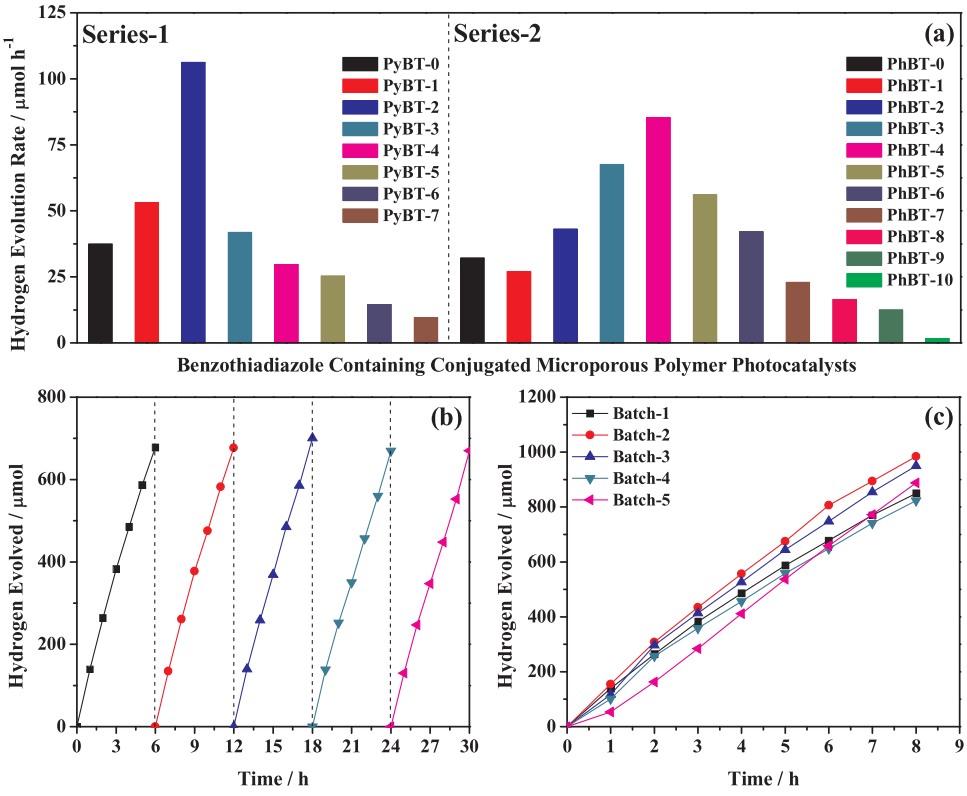

Fig. 4. (a) HER of the CMP photocatalysts with 3 wt % Pt under UV–vis light irradiation (λ > 300 nm); (b) Stability test of PyBT-2 with 3 wt% Pt from water containing 20 vol% triethanolamine over a time period of 30 h (λ > 300 nm); (c) Time course of hydrogen evolution of PyBT-2 (with 3 wt% Pt) produced from different batches in water containing 20 vol% triethanolamine under UV–vis light irradiation (λ > 300 nm).

for improving the photocatalytic performance. These profound structural effects revealed in this work offer a promising platform for efficient organic photocatalysts. Considering the wide number of donor and acceptor units, there is a wealth of opportunity for producing other D-π-A CMPs photocatalysts with enhanced photocatalytic performance by the rational selecting donor and acceptor units.

Author contributions

All authors have given approval to the final version of the manuscript.

Acknowledgments

This work was supported by the National Natural Science Foundation of China (21574077 & 21304055), the Fundamental Research Funds for the Central Universities (2016CBZ001), and the Opening Project of State Key Laboratory of Polymer Materials Engineering from Sichuan University (Grant No. sklpme2016-4-22).

Appendix A. Supplementary data

Supplementary material related to this article can be found, in the online version, at doi:https://doi.org/10.1016/j.apcatb.2018.01.073.

References

[1] R. Asahi, T. Morikawa, H. Irie, T. Ohwaki, Chem. Rev. 114 (2014) 9824–9852.
[2] J. Zhang, Y. Chen, X. Wang, Energy Environ. Sci. 8 (2015) 3092–3108.
[3] G. Zhang, Z.-A. Lan, X. Wang, Chem. Sci. 8 (2017) 5261–5274.
[4] Q. Xiang, J. Yu, M. Jaroniec, Chem. Soc. Rev. 41 (2012) 782–796.
[5] A. Kudo, Y. Miseki, Chem. Soc. Rev. 38 (2009) 253–278.
[6] X. Chen, S. Shen, L. Guo, S.S. Mao, Chem. Rev. 110 (2010) 6503–6570.
[7] L. Liu, X. Gu, Z. Ji, W. Zou, C. Tang, F. Gao, L. Dong, J. Phys. Chem. C 117 (2013) 18578–18587.
[8] L. Liu, Z. Ji, W. Zou, X. Gu, Y. Deng, F. Gao, C. Tang, L. Dong, ACS Catal. 3 (2013) 2052–2061.
[9] W. Zou, L. Zhang, L. Liu, X. Wang, J. Sun, S. Wu, Y. Deng, C. Tang, F. Gao, L. Dong, Appl. Catal. B: Environ. 181 (2016) 495–503.
[10] J. Liu, Y. Liu, N. Liu, Y. Han, X. Zhang, H. Huang, Y. Lifshitz, S.-T. Lee, J. Zhong, Z. Kang, Science 347 (2015) 970–974.
[11] H. Yu, R. Shi, Y. Zhao, G.I.N. Waterhouse, L.-Z. Wu, C.-H. Tung, T. Zhang, Adv. Mater. 28 (2016) 9454–9477.
[12] K. Sakaushi, M. Antonietti, Acc. Chem. Res. 48 (2015) 1591–1600.
[13] V.S. Vyas, V.W.-h. Lau, B.V. Lotsch, Chem. Mater. 28 (2016) 5191–5204.
[14] G. Zhang, Z.-A. Lan, X. Wang, Angew. Chem. Int. Ed. 55 (2016) 15712–15727.
[15] Y.L. Wong, J.M. Tobin, Z. Xu, F. Vilela, J. Mater. Chem. A 4 (2016) 18677–18686.
[16] E. Lanzarini, M.R. Antognazza, M. Biso, A. Ansaldo, L. Laudato, P. Bruno, P. Metrangolo, G. Resnati, D. Ricci, G. Lanzani, J. Phys. Chem. C 116 (2012) 10944–10949.
[17] S. Yanagida, A. Kabumoto, K. Mizumoto, C. Pac, K. Yoshinob, J. Chem. Soc. Chem. Commun. 8 (1985) 474–475.
[18] T. Shibata, A. Kabumoto, T. Shiragami, O. Ishitani, C. Pac, S. Yanagida, J. Phys. Chem. 94 (1990) 2068–2076.
[19] T. Yamamoto, Y. Yoneda, T. Maruyama, J. Chem. Soc. Chem. Commun. 15 (1992) 1652–1654.
[20] T. Maruyama, T. Yamamoto, J. Phys. Chem. B 101 (1997) 3806–3810.
[21] L. Li, R.G. Hadt, S. Yao, W.-Y. Lo, Z. Cai, Q. Wu, B. Pandit, L.X. Chen, L. Yu, Chem. Mater. 28 (2016) 5394–5399.
[22] X. Wang, K. Maeda, A. Thomas, K. Takanabe, G. Xin, J.M. Carlsson, K. Domen, M. Antonietti, Nat. Mater. 8 (2009) 76–80.
[23] Q. Han, B. Wang, J. Gao, Z. Cheng, Y. Zhao, Z. Zhang, L. Qu, ACS Nano 10 (2016) 2745–2751.
[24] Q. Liang, Z. Li, X. Yu, Z.-H. Huang, F. Kang, Q.-H. Yang, Adv. Mater. 27 (2015) 4634–4639.
[25] W. Cheng, H. Su, F. Tang, W. Che, Y. Huang, X. Zheng, T. Yao, J. Liu, F. Hu, Y. Jiang, Q. Liu, S. Wei, J. Mater. Chem. A 5 (2017) 19649–19655.
[26] Q. Tay, P. Kanhere, C.F. Ng, S. Chen, S. Chakraborty, A.C.H. Huan, T.C. Sum, R. Ahuja, Z. Chen, Chem. Mater. 27 (2015) 4930–4933.
[27] J. Chen, D. Zhao, Z. Diao, M. Wang, S. Shen, Sci. Bull. 61 (2016) 292–301.
[28] W. Zou, Y. Shao, Y. Pu, Y. Luo, J. Sun, K. Ma, C. Tang, F. Gao, L. Dong, Appl. Catal. B: Environ. 218 (2017) 51–59.
[29] H. Yu, R. Shi, Y. Zhao, T. Bian, Y. Zhao, C. Zhou, G.I.N. Waterhouse, L.-Z. Wu, C.-H. Tung, T. Zhang, Adv. Mater. 29 (2017) 1605148.
[30] C. Ye, J.-X. Li, Z.-J. Li, X.-B. Li, X.-B. Fan, L.-P. Zhang, B. Chen, C.-H. Tung, L.-Z. Wu, ACS Catal. 5 (2015) 6973–6979.
[31] T. Xiong, W. Cen, Y. Zhang, F. Dong, ACS Catal. 6 (2016) 2462–2472.
[32] Z. Mao, J. Chen, Y. Yang, D. Wang, L. Bie, B.D. Fahlman, ACS Appl. Mater. Interfaces 9 (2017) 12427–12435.
[33] R.S. Sprick, J.-X. Jiang, B. Bonillo, S. Ren, T. Ratvijitvech, P. Guiglion, M.A. Zwijnenburg, D.J. Adams, A.I. Cooper, J. Am. Chem. Soc. 137 (2015) 3265–3270.
[34] L. Li, Z. Cai, Q. Wu, W.-Y. Lo, N. Zhang, L.X. Chen, L. Yu, J. Am. Chem. Soc. 138 (2016) 7681–7686.
[35] C. Yang, B.C. Ma, L. Zhang, S. Lin, S. Ghasimi, K. Landfester, K.A.I. Zhang, X. Wang,

Angew. Chem. Int. Ed. 55 (2016) 9202–9206.
[36] V.S. Vyas, B.V. Lotsch, Nature 521 (2015) 41–42.
[37] R.S. Sprick, B. Bonillo, M. Sachs, Rob. Clowes, J.R. Durrant, D.J. Adamsa, A.I. Cooper, Chem. Commun. 52 (2016) 10008–10011.
[38] R.S. Sprick, B. Bonillo, R. Clowes, P. Guiglion, N.J. Brownbill, B.J. Slater, F. Blanc, M.A. Zwijnenburg, D.J. Adams, A.I. Cooper, Angew. Chem. Int. Ed. 55 (2016) 1792–1796.
[39] L. Li, W.-Y. Lo, Z. Cai, N. Zhang, L. Yu, Macromolecules 49 (2016) 6903–6909.
[40] Y. Xu, N. Mao, S. Feng, C. Zhang, F. Wang, Y. Chen, J. Zeng, J.-X. Jiang, Macromol. Chem. Phys. 218 (2017) 1700049.
[41] Y. Xu, C. Zhang, P. Mu, N. Mao, X. Wang, Q. He, F. Wang, J.-X. Jiang, Sci. China Chem. 60 (2017) 1075–1083.
[42] P.B. Pati, G. Damas, L. Tian, D.L.A. Fernandes, L. Zhang, I.B. Pehlivan, T. Edvinsson, C.M. Araujo, H. Tian, Energy Environ. Sci. 10 (2017) 1372–1376.
[43] J. Bi, W. Fang, L. Li, J. Wang, S. Liang, Y. He, M. Liu, L. Wu, Macromol. Rapid Commun. 36 (2015) 1799–1805.
[44] L. Stegbauer, K. Schwinghammer, B.V. Lotsch, Chem. Sci. 5 (2014) 2789–2793.
[45] S. Bernhardt, M. Kastler, V. Enkelmann, M. Baumgarten, K. Müllen, Chem. Eur. J. 12 (2006) 6117–6128.
[46] P. Sonar, T.R.B. Foong, S.P. Singh, Y. Li, A. Dodabalapur, Chem. Commun. 48 (2012) 8383–8385.
[47] M.N. Eliseeva, L.T. Scott, J. Am. Chem. Soc. 134 (2012) 15169–15172.
[48] X. Wang, P. Mu, C. Zhang, Y. Chen, J. Zeng, F. Wang, J.-X. Jiang, ACS Appl. Mater. Interfaces 9 (2017) 20779–20786.
[49] C. Zhang, Y. He, P. Mu, X. Wang, Q. He, Y. Chen, J. Zeng, F. Wang, Y. Xu, J.-X. Jiang, Adv. Funct. Mater. 28 (2018) 1705432.
[50] L. Li, Z. Cai, Polym. Chem. 7 (2016) 4937–4943.
[51] X. Fan, L. Zhang, R. Cheng, M. Wang, M. Li, Y. Zhou, J. Shi, ACS Catal. 5 (2015) 5008–5015.
[52] Z.-L. Wu, C.-H. Wang, B. Zhao, J. Dong, F. Lu, W.-H. Wang, W.-C. Wang, G.-J. Wu, J.-Z. Cui, P. Cheng, Angew. Chem. Int. Ed. 55 (2016) 4938–4942.
[53] D. Wang, Z.-P. Liu, W.-M. Yang, ACS Catal. 7 (2017) 2744–2752.
[54] F. He, G. Chen, Y. Yu, S. Hao, Y. Zhou, Y. Zheng, ACS Appl. Mater. Interfaces 6 (2014) 7171–7179.
[55] S. Kuecken, A. Acharjya, L. Zhi, M. Schwarze, R. Schomäcker, A. Thomas, Chem. Commun. 53 (2017) 5854–5857.
[56] D.-L. Jiang, C.-K. Choi, K. Honda, W.-S. Li, T. Yuzawa, T. Aida, J. Am. Chem. Soc. 126 (2004) 12084–12089.
[57] M.G. Schwab, M. Hamburger, X. Feng, J. Shu, H.W. Spiess, X. Wang, M. Antonietti, K. Müllen, Chem. Commun. 46 (2010) 8932–8934.
[58] S. Wang, X. Yang, H. Hou, X. Ding, S. Li, F. Deng, Y. Xiang, H. Chen, Catal. Sci. Technol. 7 (2017) 418–426.
[59] H.-J. Hou, X.-H. Zhang, D.-K. Huang, X. Ding, S.-Y. Wang, X.-L. Yang, S.-Q. Li, Y.-G. Xiang, H. Chen, Appl. Catal. B: Environ. 203 (2017) 563–571.
[60] G. Mukherjee, J. Thote, H.B. Aiyappa, S. Kandambeth, S. Banerjee, K. Vanka, R. Banerjee, Chem. Commun. 53 (2017) 4461–4464.
[61] J. Ran, J. Zhang, J. Yu, M. Jaroniec, S.Z. Qiao, Chem. Soc. Rev. 43 (2014) 7787–7812.
[62] S. Chen, S. Shen, G. Liu, Y. Qi, F. Zhang, C. Li, Angew. Chem. Int. Ed. 54 (2015) 3047–3051.
[63] J. Ran, T.Y. Ma, G. Gao, X.-W. Du, S.Z. Qiao, Energy Environ. Sci. 8 (2015) 3708–3717.
[64] Z.-A. Lan, Y. Fang, Y. Zhang, X. Wang, Angew. Chem. Int. Ed. 57 (2018) 470–474.